

AD/A-002 478

STUDIES OF THE ACOUSTIC WAVES FORMED  
IN AN ELECTRIC DISCHARGE CO LASER  
CAVITY

P. I. Shen, et al

Northrop Research and Technology Center

Prepared for:

Office of Naval Research  
Advanced Research Projects Agency

November 1974

DISTRIBUTED BY:

**NTIS**

National Technical Information Service  
U. S. DEPARTMENT OF COMMERCE

UNCLASSIFIED

SECURITY CLASSIFICATION OF THIS PAGE (When Data Entered)

AD/A002 478

REPORT DOCUMENTATION PAGE		READ INSTRUCTIONS BEFORE COMPLETING FORM
1. REPORT NUMBER NRTC 74-58R	2. GOVT ACCESSION NO.	3. RECIPIENT'S CATALOG NUMBER
4. TITLE (and Subtitle) Studies of the Acoustic Waves Formed in an Electric Discharge CO Laser Cavity		5. TYPE OF REPORT & PERIOD COVERED Special Technical Report
		6. PERFORMING ORG. REPORT NUMBER NRTC 74-58R
7. AUTHOR(s) P. I. Shen and W. S. Griffin		8. CONTRACT OR GRANT NUMBER(s) N00014-72-C-0043
9. PERFORMING ORGANIZATION NAME AND ADDRESS Northrop Research and Technology Center 3401 West Broadway Hawthorne, California 90250		10. PROGRAM ELEMENT, PROJECT, TASK AREA & WORK UNIT NUMBERS ARPA Order No. 1806
11. CONTROLLING OFFICE NAME AND ADDRESS Advanced Research Projects Agency 1400 Wilson Blvd. Arlington, Virginia 22209		12. REPORT DATE November 1974
		13. NUMBER OF PAGES 42 48
14. MONITORING AGENCY NAME & ADDRESS (if different from Controlling Office) Office of Naval Research Department of the Navy Arlington, Virginia 22217		15. SECURITY CLASS. (of this report) Unclassified
		15a. DECLASSIFICATION DOWNGRADING SCHEDULE -
16. DISTRIBUTION STATEMENT (of this Report) None		
17. DISTRIBUTION STATEMENT (of the abstract entered in Block 20, if different from Report) None		
18. SUPPLEMENTARY NOTES None		
19. KEY WORDS (Continue on reverse side if necessary and identify by block number) Electric Discharge Lasers Acoustics Waves Plasma Heating		
20. ABSTRACT (Continue on reverse side if necessary and identify by block number) This work summarizes analytical and experimental studies of the compression and rarefaction waves which occur in a pulsed CO electric discharge laser's cavity. The one-dimensional, acoustical analysis includes localized heating around the cathode, heat transfer to the cathode, flow through both the cathode and anode, and bulk heating of the plasma. With the aid of the analysis, bulk heating rates of CO lasing mixtures were calculated for		

DD FORM 1 JAN 73 1473

EDITION OF 1 NOV 65 IS OBSOLETE

i

UNCLASSIFIED (48)

SECURITY CLASSIFICATION OF THIS PAGE (When Data Entered)

UNCLASSIFIED

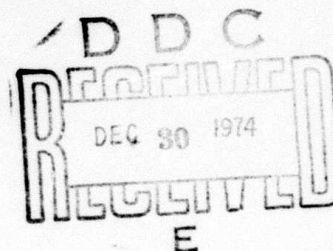
SECURITY CLASSIFICATION OF THIS PAGE(When Data Entered)

20. Abstract

various temperatures and pressures. Results from experimental studies of a Northrop pulsed CO laser were used. Heating rates are presented for Argon-CO, N<sub>2</sub>-CO, and N<sub>2</sub>.

STUDIES OF THE ACOUSTIC WAVES  
FORMED IN AN  
ELECTRIC DISCHARGE CO LASER CAVITY  
SPECIAL TECHNICAL REPORT

November 1974



Prepared by

P. I. Shen and W. S. Griffin

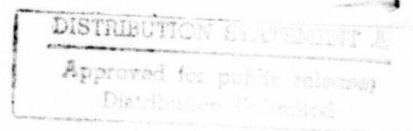
Contract N00014-72-C-0043

Sponsored by

ADVANCED RESEARCH PROJECTS AGENCY  
ARPA Order No. 1807

Monitored by

OFFICE OF NAVAL RESEARCH  
Code 421



iii.

NORTHROP CORPORATION  
Northrop Research and Technology Center  
High Power Laser Program Office  
3401 West Broadway  
Hawthorne, California 90250  
(213) 675-4611, Ext. 2821

PROGRAM IDENTIFICATION

ARPA Order No.: 1307

Program Code No.: 3E90

Name of Contractor: Northrop Corporation  
Northrop Research and Technology  
Center

Effective Date of Contract: 1 August 1971 - 30 September 1974

Amount of Contract: \$3, 550, 663. 00

Contract No.: N00014-72-C-0043

Program Manager: Dr. D. K. Rice  
(213) 675-4611, Ext. 5163

Scientific Officer: Director, Physics Program  
Physical Sciences Division  
Office of Naval Research  
Department of the Navy  
800 North Quincy Street  
Arlington, Virginia 22217

Disclaimer: The views and conclusions contained in this document are those of the authors and should not be interpreted as necessarily representing the official policies, either expressed or implied, of the Advanced Research Projects Agency or the United States Government.

Reproduction in whole or in part is permitted for any purpose of the United States Government.

## TABLE OF CONTENTS

1.0	INTRODUCTION	1
2.0	DESCRIPTION OF THE PROBLEM	3
3.0	ANALYSIS WITHOUT CATHODE FALL HEAT TRANSFER	10
3.1	Governing Equations	10
3.2	Boundary Conditions	12
3.3	General Solution	14
3.4	Cathode Wave Solution	16
3.5	Bulk Heating of the Plasma	18
3.6	Density Fluctuations in the Laser Cavity	19
4.0	ANALYSIS WITH CATHODE FALL HEAT TRANSFER	25
5.0	DETERMINATION OF BULK HEATING OF THE LASER PLASMA	35
6.0	REFERENCES	42

## 1.0 INTRODUCTION

Subsonic flow, pulsed electric discharge lasers have propagation advantages and good control over the lasing kinetics. However, the energy input to the laser gas is temporally and spatially nonuniform. This nonuniform deposition of energy into the laser cavity gas can cause pressure and rarefaction waves which, in turn, degrade the optical quality of the cavity. The formation of these waves thus places ultimate limits on the maximum pulse length, maximum repetition rate, maximum output energy per pulse, and maximum output power obtainable from pulsed EDLs.

The presence of pressure waves inside the active volumes of electric discharge lasers has been previously recognized and attacked.<sup>1, 2, 3</sup> These analyses used a Fourier series to represent the spatial distribution of the energy input and concentrated on attenuating the fundamental component. Thus, although they were used with good success in designing the acoustical absorbers for repetitively pulsed systems, they did not lend themselves well to predicting the actual density variations to be expected during the lasing pulse. Diagnosis of instantaneous heating rates was rendered difficult due to the requirement of solving for and summing a large number of the spatial Fourier components of the wave structure. In addition, they did not attack the wave formed by the intense heating in the cathode fall.

This document summarizes the results of a combined analytical/experimental effort at Northrop Corporation under Contract N00014-72-C-0043 aimed at providing improved and simplified means of predicting the pressure and

rarefaction wave structure found in pulsed electric discharge laser cavities. This analysis is addressed more to the formation of waves during and immediately after the lasing pulse as opposed to the prior work<sup>1, 2, 3</sup> which addressed the problem of attenuation of the waves after the pulse. In addition the important issue of heat transfer to the cathode from the cathode sheath has been analytically attacked and its effect is shown.

For the sake of generality of approach, a Green's function formulation was used which lends itself well to the approximations of uniform bulk heating and uniform cathode fall heating. Simple expressions are thus derived which can be used to predict the total density variations within the EDL active volume. Using the improved analysis and experimentally determined density profiles, it is feasible to predict instantaneous heating rates during the laser pulse.

## 2.0 DESCRIPTION OF THE PROBLEM

Figure 1 shows a typical cross section of the electric discharge laser cavities currently under study at Northrop. The optical axis is perpendicular to the paper and the electric field is parallel to it. An electron gun, at the top, ionizes the laser gas with high energy electrons while a dc sustainer field, applied between the anode and the cathode, provides the electrical power to pump the molecules to vibrationally excited states. During the pumping and optical extraction processes, heating of the gas occurs. For carbon monoxide lasers, the dominant heating process is VV. This occurs as a result of the anharmonic defect between adjacent vibrational energy levels in the gas and the fact that the vibrational energy structure is continuously adjusting during the pumping and optical extraction processes.

Appearance of this thermal energy causes the sensible temperature of the gas to rise and, initially, the pressure to rise. Since some of the boundaries of the cavity are either open or porous, cavity fluid leaks out, sending back rarefaction waves into the cavity. Extremely high local heating occurs in a thin sheath around the cathode. This intense local heating causes an additional wave structure to be formed which sends a compression wave into the cavity.

The types of laser cavities studied in this report have a porous anode through which flow is injected into the cavity. The sidewalls are nonporous and guide the fluid up towards the cathode screen. After the cathode screen, the flow is directed sideways between the sidewalls and the electron gun to a large cross sectional area manifold where it is exhausted by a pump. During typical pulse

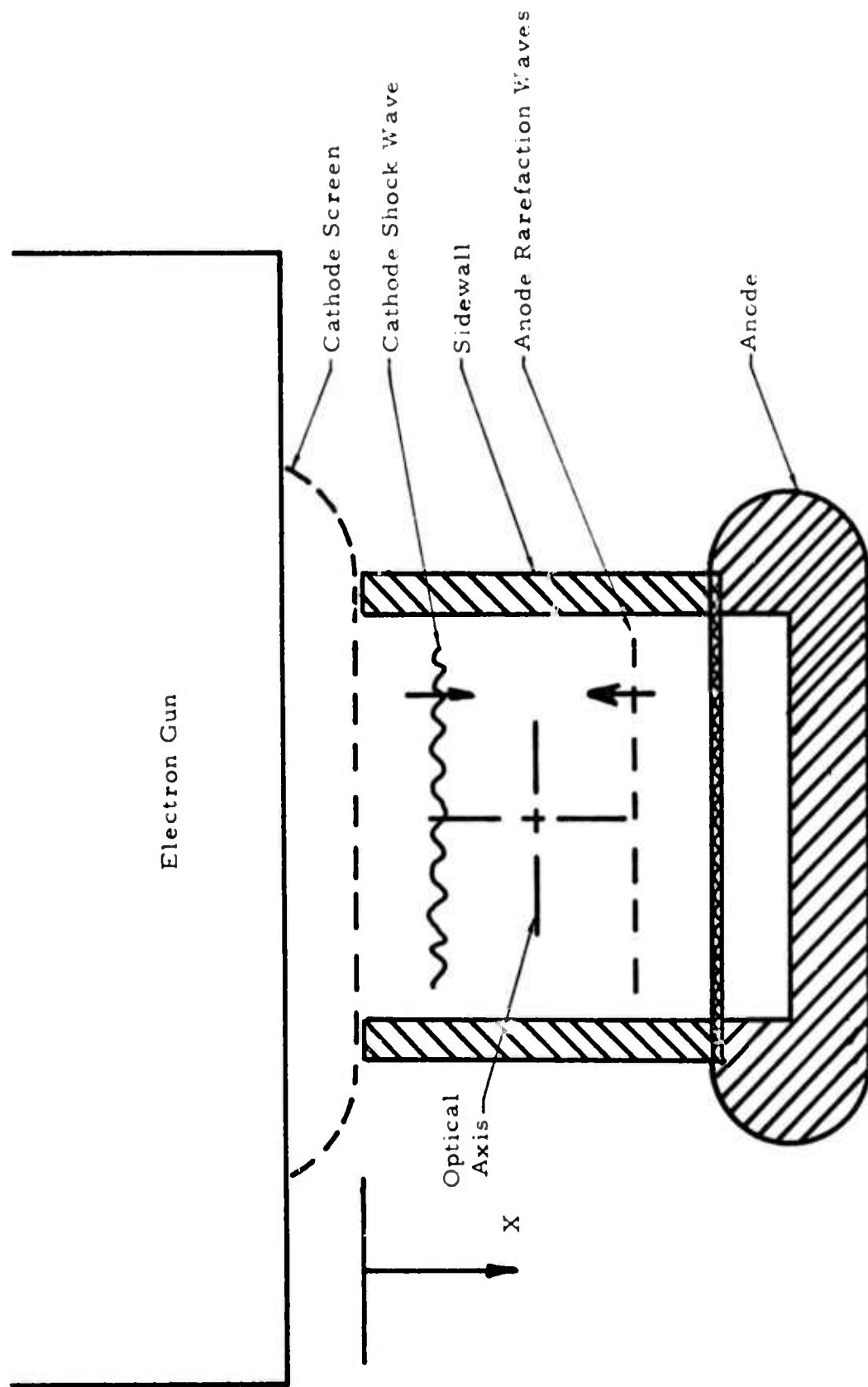


Figure 1. Illustration of the cavity acoustical model.

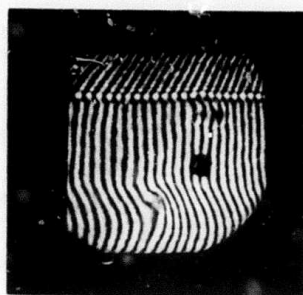
time periods ( $t < t_p$ ), the exhaust manifold may be considered to be an infinite volume. The same is not true of the channel in the anode which feeds the anode's porous upper surface, however. In the case of the anode, the flow leaking from the cavity through the anode screen will strike the bottom of the anode channel and reflect back towards the cavity, sending pressure waves into the cavity.

On the basis of the above qualitative description, one would expect the following approximate distribution of waves in the cavity during and after lasing discharge:

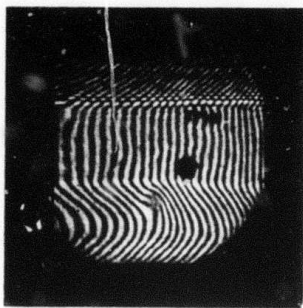
- a. From the cathode area, a sharp compression wave (due to cathode fall heating) followed by a rarefaction wave (representing leakage of cavity gas through the cathode structure).
- b. From the anode, a rarefaction wave followed by a subsequent set of compression waves caused by the finite depth of the channel underneath the anode screen.
- c. A final, sharp step compression wave on the heels of the cathode rarefaction waves that would represent the cessation of heating in the cavity ( $t > t_p$ ).

Figure 2 shows a typical Mach-Zehnder interferogram of a 1 meter length, 10 liter CO laser cavity shortly after termination of the lasing pulse.

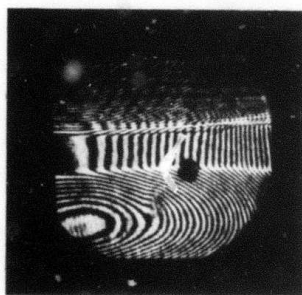
Arrangement of cavity components is the same as in Figure 1. As can be seen, the previously described wave patterns in a., b., and c., above are clearly present in the interferogram. Also to be noted are the relatively



(a)



(b)



(c)

Figure 2. Interferograms for electrically excited laser gas pumped at (a)  $135 \text{ W/cm}^3$ , (b)  $400 \text{ W/cm}^3$ , and (c)  $1250 \text{ W/cm}^3$ .

linear gradients and the small percentage perturbations in cavity density (small number of fringe shifts). A plot of the cavity density gradients would thus be expected to look somewhat like that shown in Figure 3.

Because of the relatively small percentage changes in cavity density, an acoustical treatment of the wave formation and propagation is indicated. The linear density gradients imply relatively uniform heating spatially and temporally. Thus, the analytical formulation should be adapted to this type of energy input. These two considerations point towards an acoustical analysis based on Green's functions. The Green's function approach, although quite general, is well adapted to step changes in heat rate, both spatially and temporally. The acoustical wave equations, of course, are linearized. Convolution of the Green's function solution with the actual expected spatial heating profiles is thus valid within the limitations and assumptions inherent in an acoustical analysis.

As can be seen in Figure 2, an appreciable and abrupt compression wave emanates from the cathode region. This cathode wave results from the intense heating in the cathode fall region (the plasma sheath which surrounds the cathode wires) and is large enough to cause severe density gradients in the laser cavity. Since it is heating which causes the cathode wave to be formed, it is reasonable to assume that the high temperatures thus created in the cathode sheath will also transfer appreciable amounts of thermal energy to the cathode screen wires. This heat transfer should affect the magnitude of the cathode wave. Thus, the analytical description of the cathode wave structure

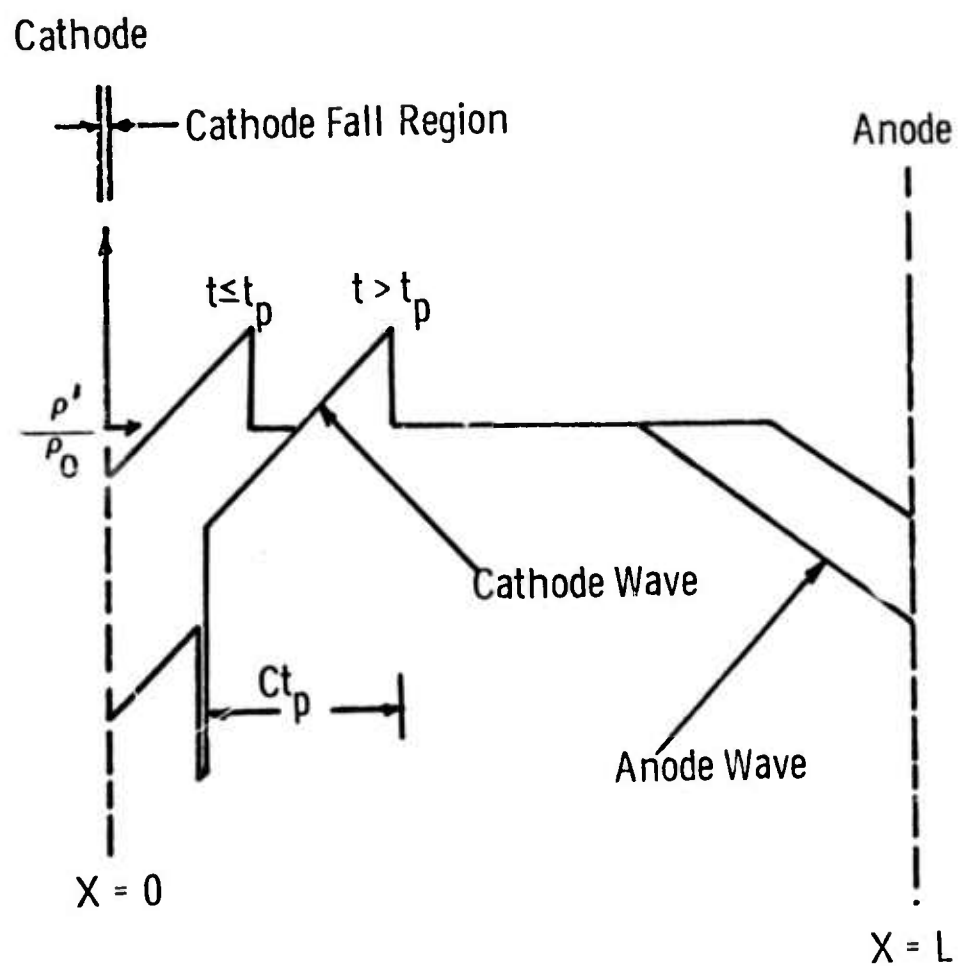


Figure 3. Expected density variations in a CO EDL cavity.

should take into account, in some manner, the effects of local cathode fall heat transfer.

The general form of the analytical description of the wave patterns thus appears to be use of Green's functions and an acoustical analysis. Heat transfer effects and local heating in the cathode fall region must be accounted for as well as porous boundaries at the top and bottom of the laser cavity. The following two sections outline the analysis and present typical results for CO lasers. The first ignores heat transfer in the cathode fall area. Although this leads to an error in the predicted results, the second analysis which includes cathode fall heat transfer shows that this error becomes quite small a short distance behind the cathode fall compression wave. The simpler zero heat transfer model can thus be used for interpretation of experimental wave patterns including bulk heating rates. Because it ignores cathode heat transfer, its results are quite easy to use.

### 3.0 ANALYSIS WITHOUT CATHODE FALL HEAT TRANSFER

Proceeding first with the zero cathode fall heat transfer case, we idealize the actual cavity geometry as shown in Figure 4. The cathode is assumed to be a screen of very high porosity and has the acoustical impedance of an open channel. The anode is idealized as a porous plate of much lower acoustical impedance.

3.1 Governing Equations. To formulate the basic equations of motion, the following assumptions are made:

- a. Small amplitude waves.
- b. Negligible convection terms.
- c. Bulk heating of the plasma and local heating of the cathode sheath are step functions in time and space.
- d. Perfect gas with constant specific heat.

With these assumptions, one may write the following one-dimensional equations of:

Continuity

$$\frac{\partial \rho'}{\partial t} + \rho \frac{\partial u'}{\partial x} = 0 \quad (1)$$

Momentum

$$\rho \frac{\partial u'}{\partial t} + \frac{\partial p'}{\partial x} = 0 \quad (2)$$

Energy

$$\rho \frac{\partial T'}{\partial t} + \left( \frac{p}{C_v} \right) \frac{\partial u'}{\partial x} = \frac{\dot{Q}}{C_v} \quad (3)$$

and State

$$p' = R[\rho T' + T \rho'] \quad (4)$$

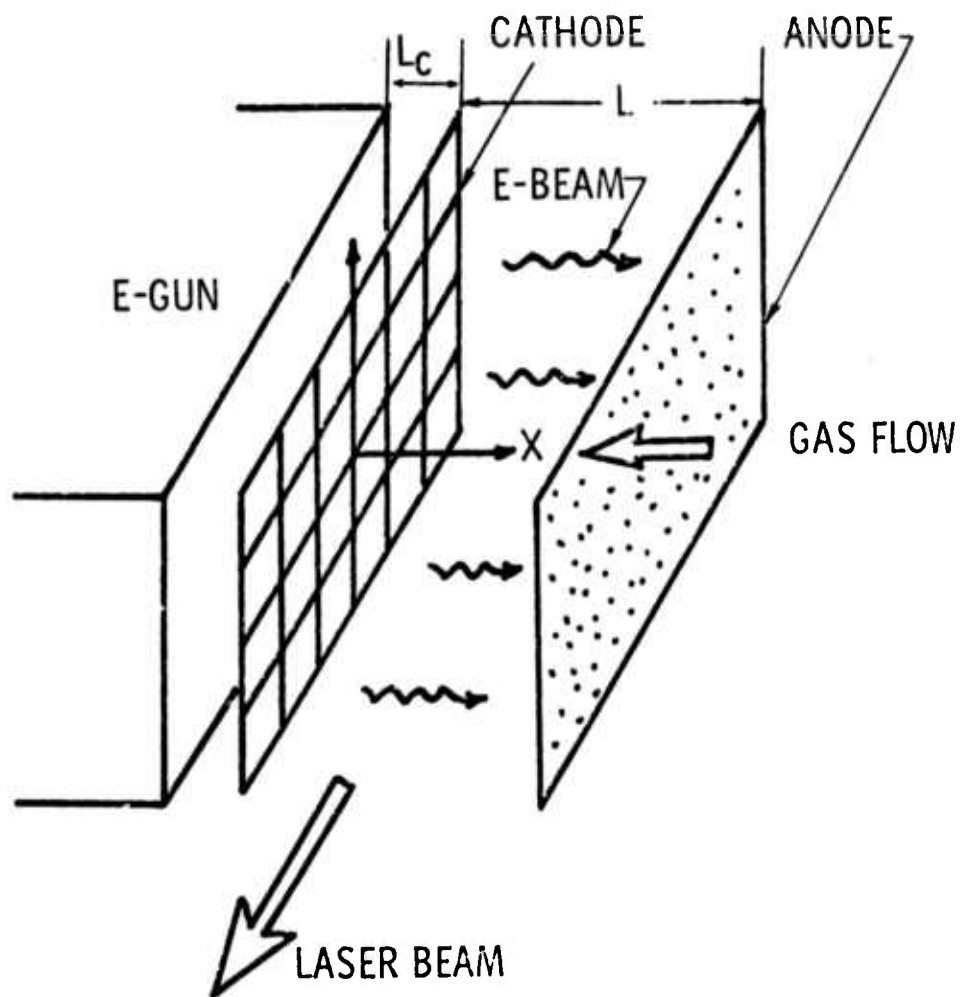


Figure 4. Idealization of the cavity of a CO laser.

where  $\rho$ ,  $u$ ,  $p$ ,  $x$ ,  $t$ ,  $T$ ,  $C_v$ , and  $\dot{Q}$  have their usual meanings of density, velocity, pressure, distance, time, temperature, specific heat at constant volume, and heat input, respectively. Primes refer to incremental changes in quantities, such as velocity and pressure, while unprimed quantities denote average values.

Combining the above equations and manipulating, one obtains the final, one-dimensional wave equation for small pressure fluctuations:

$$\frac{\partial^2 p'}{\partial t^2} - \frac{1}{c^2} \frac{\partial^2 p'}{\partial x^2} = \frac{(\gamma - 1)}{c^2} \frac{\partial \dot{Q}}{\partial t} \quad (5)$$

where, in addition to the previously defined quantities,  $\gamma$  represents the ratio of specific heat and  $c$  refers to the speed of sound in the undisturbed fluid. An important result of equation (5) is that it is linear. Hence, it is legitimate to obtain separate solutions for bulk heating of the plasma and for local heating of the cathode sheath and combine the two to obtain the complete wave solution for the cavity. A second important result of equation (5) is that pressure waves will not be generated in the cavity unless the second derivative of heat addition with respect to time is significant.

3.2 Boundary Conditions. As a second order partial differential equation, the wave equation above is subject to two initial conditions in time and two boundary conditions in space. These conditions, for both the cathode heating and for the plasma bulk heating solutions, may be written as :

Initial Conditions ( $t = 0$ , all  $x$ ):

$$p' = 0 \quad (6)$$

$$\partial p' / \partial t = (\gamma - 1) \dot{Q} \quad (7)$$

Boundary Conditions ( $t = 0^+$ )

$$\rho u' = K p' @ x = 0 \quad (8)$$

$$p' = 0 @ x = \infty \quad (9)$$

The two initial conditions refer to the fact that the initial pressure fluctuations in the laser cavity are zero (6) and that the initial rate of stored mechanical energy in the gas is equal to the initial rate of heat input (7). Customary conversion factors (J) between thermal and mechanical energy are omitted.

The two boundary conditions refer to the fact that the incremental flow through the local boundary is proportional to the incremental pressure at that boundary (8) and that the incremental pressure changes far from the flow boundary are zero (9). This latter is equivalent to saying that the gas affected by the rarefaction wave system is of finite dimension. Thus, for example, the cathode heating is presumed to occur in a small distance,  $d$ , characteristic of the cathode fall and this disturbance is not felt at distances,  $x$ , that are far removed from the fall region. Similarly, for the bulk plasma heating case, heating is presumed to occur over a finite distance,  $L$ , characteristic of the cavity dimension. At distances  $x > L$ , the analysis assumes unheated, uniform uniform laser gas ( $\dot{Q}_h = 0$ ). For distances  $x \gg L$ , pressure waves from the cavity will not have had time to propagate or will have attenuated to negligible value.

The factor,  $K$ , is a general acoustic permeability of the cathode. If the cathode has appreciable flow resistance, then  $K$  will be close to the permeability measured under steady state conditions. As the porosity of the cathode screen becomes very high,  $K$  will approach the inverse acoustic impedance of the laser gas ( $1/c$ ).

Proceeding, we may differentiate equation (8) to obtain

$$\rho \frac{\partial u'}{\partial t} = -K \frac{\partial p'}{\partial t}$$

which, when combined with momentum (2) yields

$$\frac{\partial p'}{\partial x} = K \frac{\partial p'}{\partial t} \quad (10)$$

as a second boundary condition.

3.3 General Solution. The general solution for both bulk heating of the plasma and the local cathode fall heating consists of taking the Laplace transform of wave equation

$$\tilde{p}'(x, s) = \int_0^{\infty} e^{-st} p'(x, t) dt \quad (11)$$

which yields a resulting one-dimensional wave equation in distance

$$\frac{d^2 \tilde{p}'(x, s)}{dx^2} - k^2 \tilde{p}'(x, s) = -\frac{(\gamma-1)}{c^2} s \tilde{Q} \quad (12)$$

where  $k = s/c$  and

$$\tilde{Q} = \int_0^{\infty} e^{-st} \dot{Q} dt \quad (13)$$

The solution is most conveniently accomplished by making a Green's function of (12) of the form

$$d^2 \frac{G(x/x_0)}{dx^2} - k^2 G(x/x_0) = \delta(x - x_0) \quad (14)$$

where  $\delta(x - x_0)$  is the Dirac delta function and  $x_0$  is the position of the unit source in the Green's function. The formal solution of (14) is divided into two parts:  $x < x_0$ , and  $x > x_0$ ; denoted  $G_-$  and  $G_+$ , respectively.

$$G_- = C_1^- e^{kx} + C_2^- e^{-kx} \quad (x < x_0) \quad (15a)$$

$$G_+ = C_1^+ e^{kx} + C_2^+ e^{-kx} \quad (x > x_0) \quad (15b)$$

The Green's function is required to satisfy the two continuity conditions at  $x = x_0$

$$G_-(x_0) = G_+(x_0) \quad (\text{continuous through } x_0) \quad (16a)$$

$$dG^+/dx - dG^-/dx = 1 \quad (\text{integrated value of the unit impulse}) \quad (16b)$$

and, also, the two boundary conditions, (8) and (9).

The resulting Green's functions are:

$$x < x_0$$

$$G_- = - \left[ \frac{1}{k(k + sK)} \right] \left[ k \cosh(kx) + sK \sinh(kx) \right] e^{-kx_0} \quad (17a)$$

$$x > x_0$$

$$G_+ = - \left[ \frac{1}{k(k + sK)} \right] \left[ k \cosh(kx_0) + sK \sinh(kx_0) \right] e^{-kx} \quad (17b)$$

The actual pressure distribution is the convolution of the Green's function solution (17) with respect to the spatial distribution of heating (13); i. e.,

$$\tilde{p}'(x, s) = - \left[ \frac{(\gamma - 1)}{c^2} \right] \int_0^{\infty} s \tilde{Q} G(x/x_0) dx_c \quad (18)$$

Inversion of (18) yields the final desired solution of incremental cavity pressure as a function of time and distance.

3.4 Cathode Wave Solution. Proceeding first with the cathode wave, we represent the spatial heating profile by the expressions

$$\dot{Q}(x, t) = \dot{Q}_c = \text{constant} \quad x \leq d \quad (19a)$$

$$\dot{Q}(x, t) = 0 \quad x > d \quad (19b)$$

and the temporal heating profile by the expressions

$$\dot{Q}_c = \text{constant}, \quad t \leq t_p \quad (20a)$$

$$\dot{Q}_c = 0 \quad t > t_p \quad (20b)$$

where  $t_p$  refers to the time that electrical discharge actually occurs in the laser cavity.

Substituting equations (19) and (20) into (18), integrating and inverting, yields the final expression for the pressure wave system generated by the cathode fall:

$$\begin{aligned} \frac{p_f'(x, t)}{(\gamma - 1)\dot{Q}_c} = & \frac{1}{2} U\left(t - \frac{(x-d)}{c}\right) \left[ t - \frac{x-d}{c} \right] - \frac{1-Kc}{2(1+Kc)} U\left(t - \frac{(x+d)}{c}\right) \left[ t - \frac{x+d}{c} \right] \\ & - \frac{Kc}{1+Kc} U\left(t - \frac{x}{c}\right) \left[ t - \frac{x}{c} \right] \end{aligned} \quad (21)$$

where, in addition to the previously defined quantities,  $U(\quad)$  refers to the unit step function.

The above equation may be simplified in notation by denoting

$$t^* = t/t_p \quad (22a)$$

$$x^* = x/(t_p c) \quad (22b)$$

$$p^* = p'/p \quad (22c)$$

$$\dot{Q}_c^* = (Q_c t_p)/p \quad (22d)$$

$$d^* = d/(t_p c) \quad (22e)$$

with the aid of which, equation 21 may be rewritten in the following nondimensional form:

$$p_f^*(x^*, t^*) = (\gamma - 1) \dot{Q}_c^* \left\{ \frac{1}{2} (t^* + d^* - x^*) U(t^* + d^* - x^*) - \frac{1 - Kc}{2(1 + Kc)} (t^* - d^* - x^*) U(t^* - d^* - x^*) - \frac{Kc}{1 + Kc} (t^* - x^*) U(t^* - x^*) \right\} \quad (23)$$

An interesting and important result may be obtained by letting the thickness,  $d$ , of the cathode fall region approach zero. Equation (23) is then reduced to the form

$$\lim_{d \rightarrow 0} p^* = (\gamma - 1) \frac{\dot{Q}_c^* d^*}{(1 + Kc)} \quad (23a)$$

In this limiting case, the amplitude of the cathode wave depends only upon the total power put into the cathode fall region and not upon the details of how deep the cathode sheath is or upon the local heating rate. Since the cathode sheath will be very small compared to the dimensions of the laser cavity and the overall wave structure inside it, this limiting case, with its attendant simplified analytical results, becomes a reasonable description of the cathode wave structure.

3.5 Bulk Heating of the Plasma. The relatively straight and uniformly spaced fringes of the central areas of the interferograms in Figure 2 suggest uniform heating of the plasma in the laser's active volume. Thus, for the sake of ease of analysis, we have assumed that the bulk heating of the plasma may be represented by:

$$\dot{Q} = 0 \quad \text{for } t \leq 0 \quad (24a)$$

$$\dot{Q} = \dot{Q}_h = \text{constant for } t > 0, \quad (24b)$$

Equation (24) may be substituted directly into (18) to obtain

$$\tilde{p}_c(x, s) = \lim_{d \rightarrow \infty} \int_0^d -\frac{(\gamma-1)}{c} s \tilde{Q} G(x/x_0) dx_0 = \frac{(\gamma-1)\tilde{Q}_h}{s^2} \left[ 1 - \frac{Kc e^{-\frac{sx}{c}}}{1+Kc} \right] \quad (25)$$

the inverse of which yields the following expression for the bulk heating induced expansion wave which emanates from the cathode

$$p_c^*(x^*, t^*) = (\gamma-1) \dot{Q}_h^* \left[ t^* - \frac{Kc}{1+Kc} (t^* - x^*) U(t^* - x^*) \right] \quad (26)$$

An expansion wave also emanates from the anode due to the anode's finite porosity. Denoting the effective acoustic permeability of the anode by  $K_a$  and substituting  $L-x$  in place of  $x$  above, we may write the nondimensional anode wave as

$$p_a^*(x^*, t^*) = (\gamma-1) \dot{Q}_h^* \left[ t^* - \frac{K_a c}{1+K_a c} (t^* + x^* - L) U(t^* + x^* - L) \right] \quad (27)$$

Since the differential equations are linear, the complete pressure wave system in the laser cavity may be obtained by adding the individual solutions for the cathode fall wave,  $p_f^*$ , the bulk heating induced cathode wave,  $p_c^*$ , and

the bulk heating induced anode wave,  $p_a^*$ . Combining equations (23), (26), and (27) yields the final, complete solution for the pressure fluctuations inside a pulsed electric discharge laser's cavity during and immediately after discharge:

$$\begin{aligned}
 p^*(x^*, t^*) = & (\gamma - 1) Q_h^* \left\{ t^* - \frac{Kc}{1+Kc} (t^* - x^*) U(t^* - x^*) - \frac{K_a c}{1+K_a c} (t^* + x^* - L) U(t^* + x^* - L) \right. \\
 & + \frac{Q_c^*}{Q_h^*} \left[ \frac{1}{2} (t^* + d^* - x^*) U(t^* + d^* - x^*) - \frac{(1-Kc)}{2(1+Kc)} (t^* - d^* - x^*) U(t^* - d^* - x^*) \right. \\
 & \left. \left. - \frac{Kc}{1+Kc} (t^* - x^*) U(t^* - x^*) \right] \right\} \quad (28)
 \end{aligned}$$

3.6 Density Fluctuations in the Laser Cavity. It is the density fluctuations in the cavity which are of primary concern since it is these, not pressure per se, which affect the laser beam. Fortunately, within the limits of small perturbation theory, the density fluctuations may be simply related to the previously derived pressure fluctuations. Using the first law for heat addition into the gas:

$$c_v dT = \frac{dQ}{\rho} + \frac{p}{\rho^2} d\rho \quad (29)$$

and the equation of state, the density waves will be of the form

$$d\rho = \frac{dp}{c^2} - \frac{(\gamma - 1)}{c^2} dQ_h \quad (30)$$

or, using primed quantities instead of differentials

$$\rho' = \frac{p'}{c^2} - \frac{(\gamma - 1)}{c^2} \dot{Q}_h L \quad (30a)$$

Performing the above substitution, equation (28) may be rewritten in terms of the ordered density profiles to be expected in the laser cavity:

$$\begin{aligned}
 \rho^* &= \frac{1}{\gamma} \left[ p^* - (\gamma - 1) \dot{Q}_h^* t^* \right] \\
 &= \frac{\gamma - 1}{\gamma} \dot{Q}_h^* \left\{ -\frac{Kc}{1+Kc} (t^* - x^*) U(t^* - x^*) - \frac{K_a c}{1+K_a c} (t^* + x^* - L^*) U(t^* + x^* - L^*) \right. \\
 &\quad + \frac{Q_c^*}{Q_h^*} \left[ \frac{1}{2} (t^* + d^* - x^*) U(t^* + d^* - x^*) - \frac{(1-Kc)}{2(1+Kc)} (t^* - d^* - x^*) U(t^* - d^* - x^*) \right. \\
 &\quad \left. \left. - \frac{Kc}{1+Kc} (t^* - x^*) U(t^* - x^*) \right] \right\} \quad (31)
 \end{aligned}$$

Although somewhat long, equation (31) is analytic and easily evaluated. A typical set of results is shown in Figure 5 in which normalized density,  $\rho^*$ , is plotted against normalized distance  $x^*$ , for various normalized times,  $t^*$ . The cathode is assumed to be completely porous. Hence,  $K = 1/c$ . Other assumed parameters are listed on the figure.

The cathode wave structure propagates from the left. It is composed of both the cathode sheath heating and the rarefaction wave which results from plasma bulk heating. The step increase in density results from the assumption that heating in the cathode sheath is uniformly distributed. Its amplitude measures the local energy flux,  $\dot{Q}_c d$ , into the cathode sheath. The linear slope following this step rise indicates that bulk heating of the plasma is uniform and that the acoustic impedance of the cathode is constant (that of the laser gas itself). At time periods exceeding the plasma discharge ( $t/t_p > 1.0$ ), a step decrease in the density appears. This step decrease is a negative wave produced as the local plasma sheath around the cathode disappears.

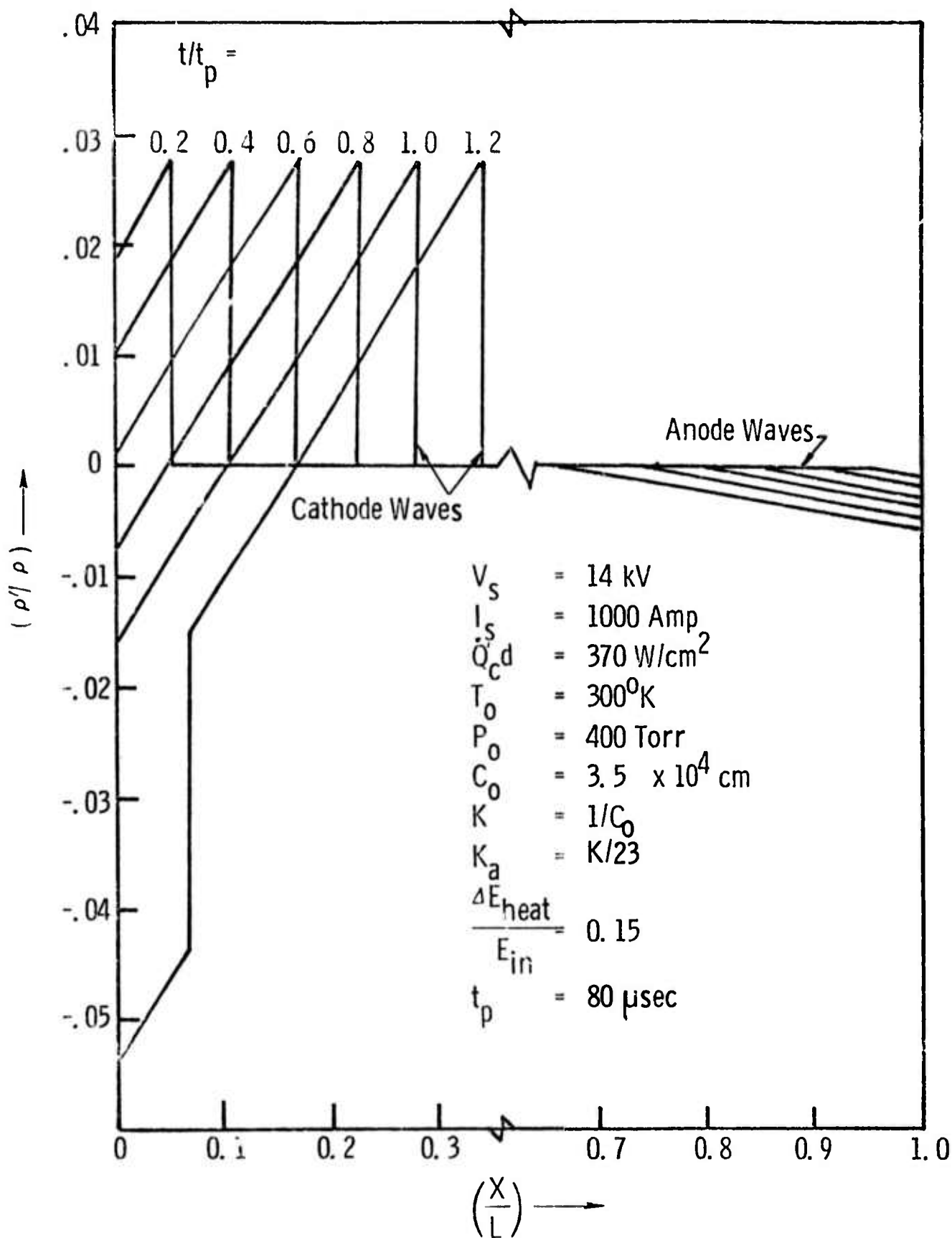


Figure 5. Theoretical density fluctuations in an electric discharge laser cavity. No heat transfer to cathode.

To be noted are the different slopes of the cathode and anode wave structures. These different density slopes reflect the difference between the assumed permeabilities for the cathode and anode (1: 1/23). As the bulk heating rate is increased, these slopes will also change as shown in Figure 6. Their ratio, however, will remain the same. The initial height of the cathode wave will, of course, remain constant as long as the assumed power input to the cathode fall remains constant.

Figure 7 shows a comparison between actual density profiles as measured in a Northrop 10 liter EDL and those predicted by this zero heat transfer analysis. (A heating rate of 15% of input power was assumed.) The slopes of the wave-fronts and their propagation into the cavity compare, in the case shown, within a few percent. The main region of uncertainty appears to be in the front of the cathode wave which the interferogram is not able to resolve.

This agreement between experiment and theory is rewarding since, as previously stated, large amounts of heat transfer to the cathode screen should occur which the present analysis neglects. Thus, this simplified analysis should be valid for interpretation of the interferograms of EDL discharges and resultant predictions of instantaneous bulk heating rates. It is, however, important to know the errors and approximations introduced by neglecting heat transfer to the cathode screen wire. The following section briefly outlines the complete analysis including cathode screen heat transfer and points out the essential differences which result.

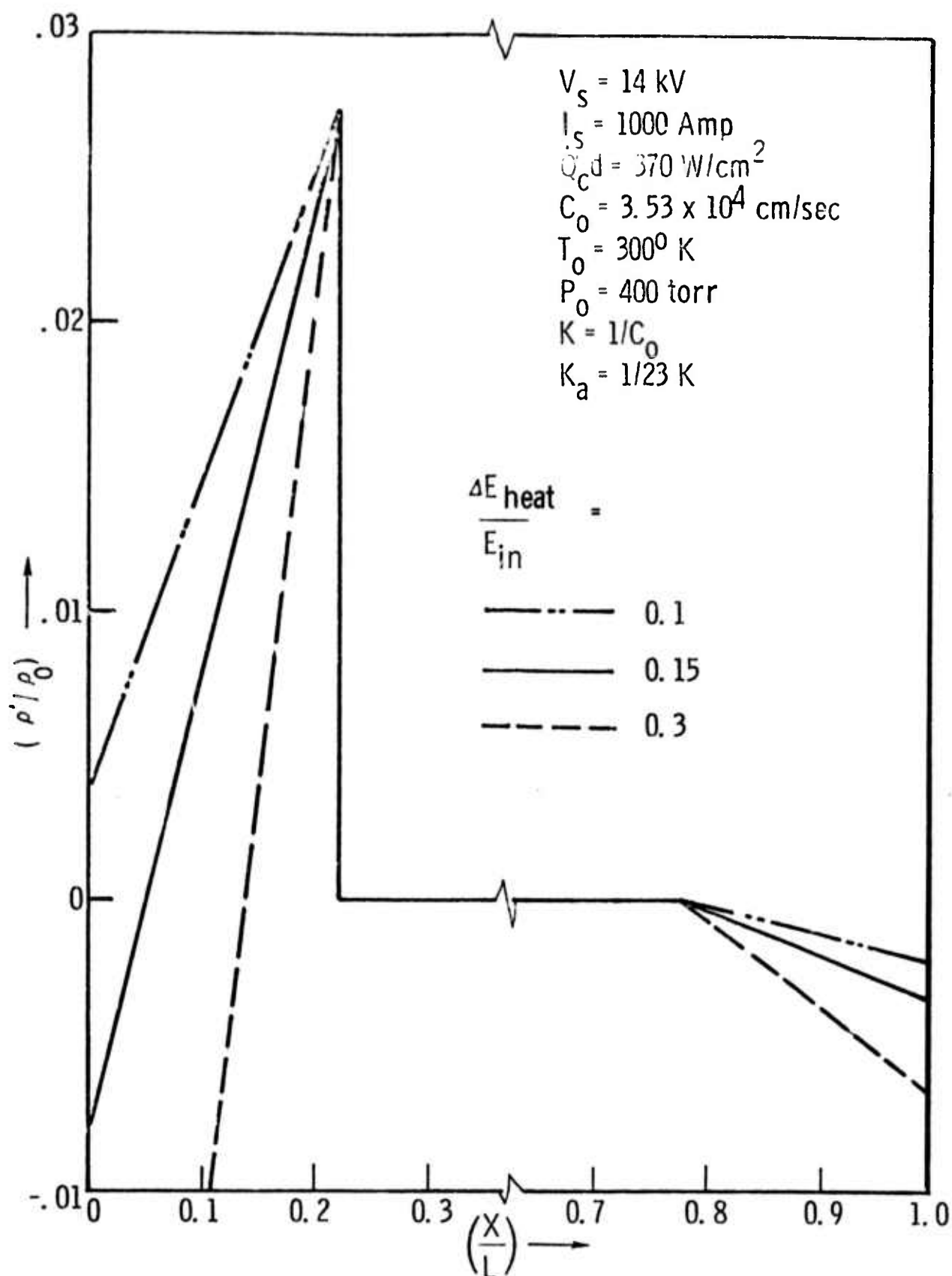


Figure 6. Illustration of the effect of changing the bulk heating ratio. Zero heat transfer to the cathode.

# DENSITY VARIATIONS PRODUCED BY CATHODE AND ANODE WAVES

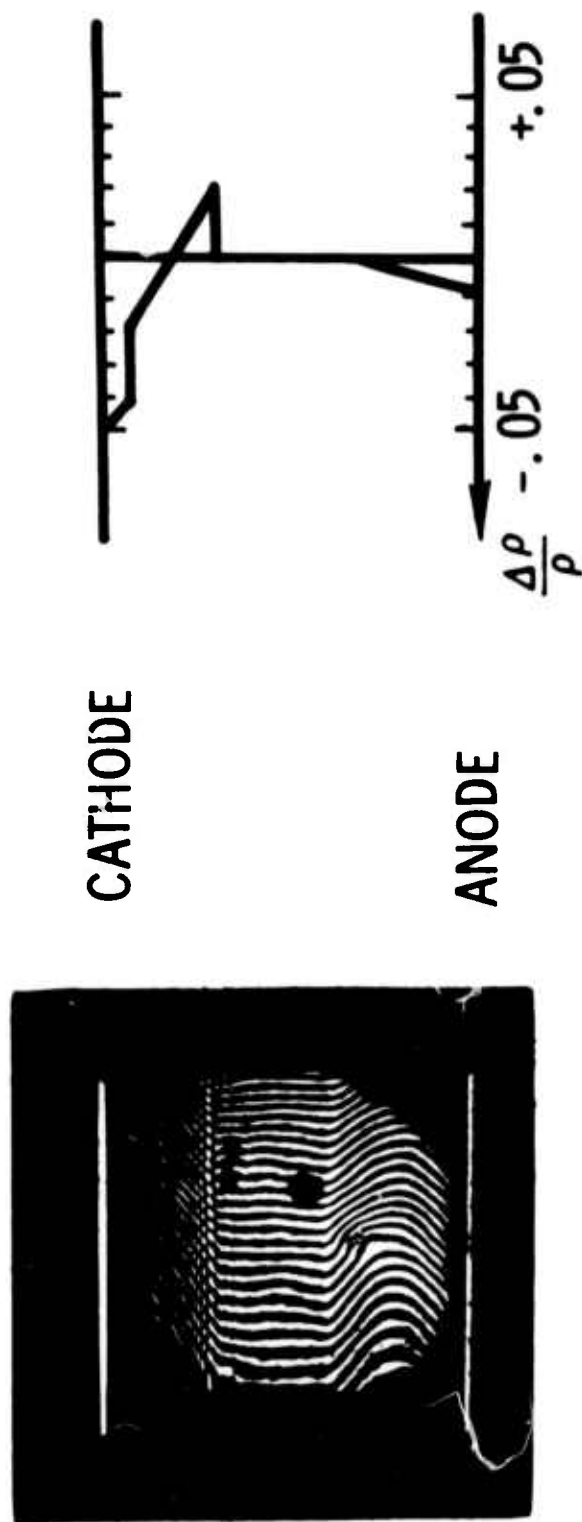


Figure 7. Comparison of the experimental and theoretically predicted density variations in a CO electric discharge laser. Zero heat transfer to the cathode assumed.

#### 4.0 ANALYSIS WITH CATHODE FALL HEAT TRANSFER

As stated earlier, high local heating rates and possible high temperatures are to be expected in the plasma sheath which surrounds the cathode wires.

As an example, one may assume a typical cathode fall of roughly

$$V_c = 370V$$

a sheath thickness of

$$d = 0.1 \text{ mm} = 0.01 \text{ cm}$$

and an average current density of

$$I/A = 1.0A/cm^2$$

Actual local current densities on the individual cathode screen wires will, of course, be much higher since their area is not spread uniformly over the entire discharge. Assuming nitrogen/CO for the gas mixture, a 100 microsecond pulse, and an average pressure of 400 Torr, one then calculates a typical, average sheath heating rate

$$\dot{Q}_c = (\dot{Q}_c d)/d = 370/(0.01) = 37,000W/cm^3$$

and a theoretical maximum temperature rise, assuming a 100 microsecond pulse, of

$$T_{\max} = \dot{Q}_c / (\rho C_v) = \frac{37,000}{(0.6 \times 10^{-3})(0.718)} = 8,550^\circ C$$

where  $\rho$  is the nominal gas density and  $C_v$  is the gas specific heat at constant volume.

This high temperature rise cannot exist in practice. Using nominal gas thermal conductivities, half the cathode fall thickness as a typical distance, one calculates, at the end of a 100 microsecond discharge, heat transfer

rates to the cathode that are in excess of the input power to the cathode fall itself. It is thus apparent that heat transfer to the cathode wires is significant and will substantially alter the details of the compression wave generated by the cathode fall.

Qualitatively, one may a priori estimate the influence of cathode sheath heat transfer. At the beginning of the discharge, when temperatures are low, heat transfer effects should be insignificant. Thus, the initial height of the compression wave emanating from the cathode should remain unchanged. At the end of the laser discharge, when adiabatic temperatures would be very high, heat transfer effects should dominate and the cathode fall compression wave should be considerably weakened. Thus, one would expect the composite density profile, including the effects of heat transfer, to look much like that shown in Figures 5 and 6 except that the slope behind the advancing compression wave on the left hand side of the figure would now not be constant. Hopefully, the change in slope should die out relatively quickly and one would be left with a slope characteristic of the impedance of the gas on the E-gun side of the cathode. Results at that point would be identical with those shown in Figures 5 and 6.

To analyze the cathode fall produced compression wave with heat transfer, we must write the full, linearized energy equation

$$\rho \frac{\partial T'}{\partial t} + \frac{p}{C_v} \frac{\partial u'}{\partial x} = \frac{\dot{Q}}{C_v} + \frac{\lambda}{C_v} \left( \frac{\partial^2 T'}{\partial x^2} \right) \quad (32)$$

This, when combined with the equations of continuity, momentum, and state, (equations (1), (2), and (4), respectively), yields a modified pressure wave equation which accounts for heat transfer:

$$\frac{\partial^2 p'}{\partial t^2} - c^2 \frac{\partial^2 p'}{\partial x^2} = (\gamma - 1) \frac{\partial \dot{Q}}{\partial t} + (\gamma - 1) \frac{\partial}{\partial t} \left( \frac{\partial^2 T'}{\partial x^2} \right) \quad (33)$$

As can be seen, equation (33) is identical to the adiabatic wave equation except for a temperature gradient term on the right hand side. Unfortunately, this temperature term is not decoupled from the pressure terms on the left hand side of the equation. The simplified Green's function approach is no longer appropriate.

This dilemma may be resolved by assuming that heat transfer effects are important only in the cathode sheath and that this distance is very small compared to the characteristic dimensions of the laser cavity and the resultant gross wave structure. By so doing, one is then able to obtain a separate approximate solution for the conduction dominated heat transfer temperature profiles in the cathode sheath and substitute these profiles into the temperature term on the right hand side of (33). Since the obtained temperature profiles will be a function of the input heating rate only, the wave equation again becomes explicit in pressure and may be solved in the same manner as used for the adiabatic case.

Proceeding in this manner, we analyze the temperatures within the cathode sheath by making the following assumptions:

- a. The surface temperature of the cathode wires does not change appreciably during the discharge time period; and
- b. Convection terms can be neglected in the sheath region.

The first assumption may be justified by making a simple, one-dimensional slab heating calculation. Because of its much higher density, the temperature rise on the cathode wires' surface required to absorb the cathode fall heat transfer is quite minimal - in the order of a few degrees centigrade. The second assumption is made primarily to ease the analysis. The resultant analytical solution is, however, consistent with this assumption and indicates that heat transfer effects outweigh convective work in the cathode fall plasma sheath.

With the aid of the above assumptions, the energy equation for the cathode fall may be written

$$\rho C_v \frac{\partial T'}{\partial t} = \lambda \frac{\partial^2 T'}{\partial x^2} + \dot{Q} \quad (34)$$

This energy equation differs from that previously used (equation (3)) by neglecting convective mechanical work ( $p(du/dx)/C_v$ ) and substituting, in its place, conductive heat transport. By so doing, the energy equation becomes decoupled from pressure terms and hence may be solved separately from the wave equation.

The solution of (34) is most conveniently accomplished with the aid of Green's functions. Boundary conditions for the solution are:

$$T' = 0 \quad @ \quad x = 0, \quad \text{all } t$$

$$T' = 0 \quad @ \quad t = 0, \quad \text{all } x$$

$$T' = 0 \quad @ \quad x \rightarrow \infty$$

Taking the Laplace transform of (34) we obtain

$$\frac{\partial^2 \tilde{T}}{\partial x^2} - \beta^2 \tilde{T} = -\frac{\tilde{Q}}{\lambda} \quad (35)$$

where  $\lambda$  is the gas thermal conductivity and  $\beta$  is the expression

$$\beta^2 = \frac{\rho C_v s}{\lambda} = s/\alpha \quad (36)$$

The resulting Green's function is then found to be

$$\begin{aligned} G_t^- &= -\sqrt{\alpha/s} \exp[-x_0/\sqrt{\alpha/s}] \sinh(\sqrt{s/\alpha} x) & x < x_0 \\ G_t^+ &= -\sqrt{\alpha/s} \exp[-x/\sqrt{\alpha/s}] \sinh(\sqrt{s/\alpha} x_0) & x > x_0 \end{aligned} \quad (37)$$

and the resulting temperature profile is given by the expressions

$$\begin{aligned} x < d \\ \tilde{T}^-(x, s) &= -\frac{\dot{Q}_c}{\lambda s^2} \alpha \left[ \exp[-\sqrt{s/\alpha} x] - 1 + \frac{1}{2} \exp[\sqrt{s/\alpha} (x-d)] \right. \\ &\quad \left. - \frac{1}{2} \exp[-\sqrt{s/\alpha} (x+d)] \right] \end{aligned} \quad (38a)$$

$$\begin{aligned} x > d \\ \tilde{T}^+(x, s) &= -\frac{\dot{Q}_c}{\lambda s^2} \alpha \exp[-\sqrt{s/\alpha} x] \left[ \cosh(\sqrt{s/\alpha} d) - 1 \right] \end{aligned} \quad (38b)$$

As can be seen above, the conduction dominated temperature profiles in the cathode sheath are a function, solely, of the cathode fall heating rate,  $\dot{Q}_c$ . Furthermore, they die out very rapidly - in a distance characteristic of the

cathode fall depth,  $d$ . Thus, using the previously described artifice of substituting the temperature profiles obtained above into the wave equation (33), one obtains an explicit wave equation with the same Green's functions as obtained for the adiabatic solution. The resultant approximate solution for the cathode fall compression wave with heat transfer effects then can be obtained by convolving the adiabatic Green's functions with the forcing term on the right hand side of (33):

$$\tilde{p}(x, s) = - \frac{(\gamma - 1)}{c^2} \int_0^{\infty} \left( s \tilde{Q} - \lambda s \frac{\partial^2 \tilde{T}}{\partial x^2} \right) G(x/x_0) dx_0 \quad (39)$$

Proceeding with the indicated integration, we obtain for distances  $x > d$ ,

$$\begin{aligned} \tilde{p}(x, s) = & - \frac{(\gamma - 1)}{c^2} \left\{ \int_0^d \dot{Q}_c G^+ dx_0 + \lambda s \int_0^d G^+ \frac{d^2 \tilde{T}^-}{dx^2} dx_0 + \lambda s \int_d^x G^+ \frac{d^2 \tilde{T}^+}{dx^2} dx_0 \right. \\ & \left. + \lambda s \int_x^{\infty} G^- \frac{d^2 \tilde{T}^+}{dx^2} dx_0 \right\} \quad (40) \end{aligned}$$

For simplicity we assume that

$$\frac{\alpha s}{c^2} \ll 1 \quad (41)$$

with the aid of which equation (40) may be integrated to obtain

$$\begin{aligned} \frac{\tilde{p}}{(\gamma - 1) \dot{Q}_c} = & \frac{1}{(1 + Kc)} \frac{e^{-kx}}{s} \left[ \frac{1 + Kc}{2} e^{kd} - \frac{(1 - Kc)}{2} e^{-kd} - Kc \right] \\ & + \frac{1}{(1 + Kc)} \sqrt{\alpha/c^2} \left[ \left( \frac{1}{s^{3/2}} \right) \exp[-sx/c - \sqrt{s/\alpha} d] - \frac{1}{s^{3/2}} \exp[-sx/c] \right] \\ & - \frac{\alpha}{2s c^2} \left[ \exp[-\sqrt{s/\alpha} (x-d)] + \exp[-\sqrt{s/\alpha} (x+d)] - 2 \exp[-\sqrt{s/\alpha} x] \right] \\ & - \exp[-s(x-d)/c] + \left( \frac{1 - Kc}{1 + Kc} \right) \exp[-s(x+d)/c] + \left( \frac{2}{s} \right) \left( \frac{Kc}{1 + Kc} \right) \exp\left(-\frac{sx}{c}\right) \quad (42) \end{aligned}$$

The inverse Laplace transform of (42) may be separated into two parts: the previously obtained adiabatic wave solution (equation (28)) and a solution which includes the effect of cathode fall heat transfer. This latter solution is denoted  $p_h^*$  and is given below in equation (43).

$$\begin{aligned}
 p_h^* = \frac{\dot{Q}_c^*}{\dot{Q}_h^*} & \left\{ \frac{\sqrt{\alpha^*}}{(1+Kc)} \left[ \sqrt{\frac{4(t^* - x^*)}{\pi}} \exp\left[-d^{*2}/4\alpha^*(t^* - x^*)\right] - \sqrt{t^* - x^*} U(t^* - x^*) \right. \right. \\
 & - \frac{d^*}{\sqrt{\alpha^*}} \operatorname{erfc}\left(\frac{d^*}{\sqrt{4\alpha^*(t^* - x^*)}}\right) \Big] - \alpha^* \left[ \frac{1}{2} \operatorname{erfc}\left(\frac{x^* - d^*}{\sqrt{4\alpha^* t^*}}\right) + \frac{1}{2} \operatorname{erfc}\left(\frac{x^* + d^*}{\sqrt{4\alpha^* t^*}}\right) \right. \\
 & - \operatorname{erfc}\left(\frac{x^*}{\sqrt{4\alpha^* t^*}}\right) - \frac{1}{2} U(t^* + d^* - x^*) + \frac{1}{2} \left( \frac{1 - Kc}{1 + Kc} \right) U(t^* - x^* - d^*) \\
 & \left. \left. + \frac{Kc}{1 + Kc} U(t^* - x^*) \right] \right\} \quad (43)
 \end{aligned}$$

where

$$\alpha^* = \frac{\alpha}{c^2 \tau_p} \quad \text{and} \quad \alpha = \frac{\lambda}{C_v} \quad (44)$$

and  $U(\ )$  is the previously described unit step function.

To illustrate the effects of cathode sheath heat transfer, the complete pressure wave equation [(43) plus the adiabatic solution (28)] is plotted in Figure 8. Figure 9 plots the corresponding density profile. Several important results stand out. First, looking at the zero cathode porosity case ( $K = 0$ ), it is seen that the initial height of the cathode wave is unattenuated by heat transfer. This is an expected result since, at  $t = 0$ , no gas heating has occurred and, hence, no heat transfer could take place.

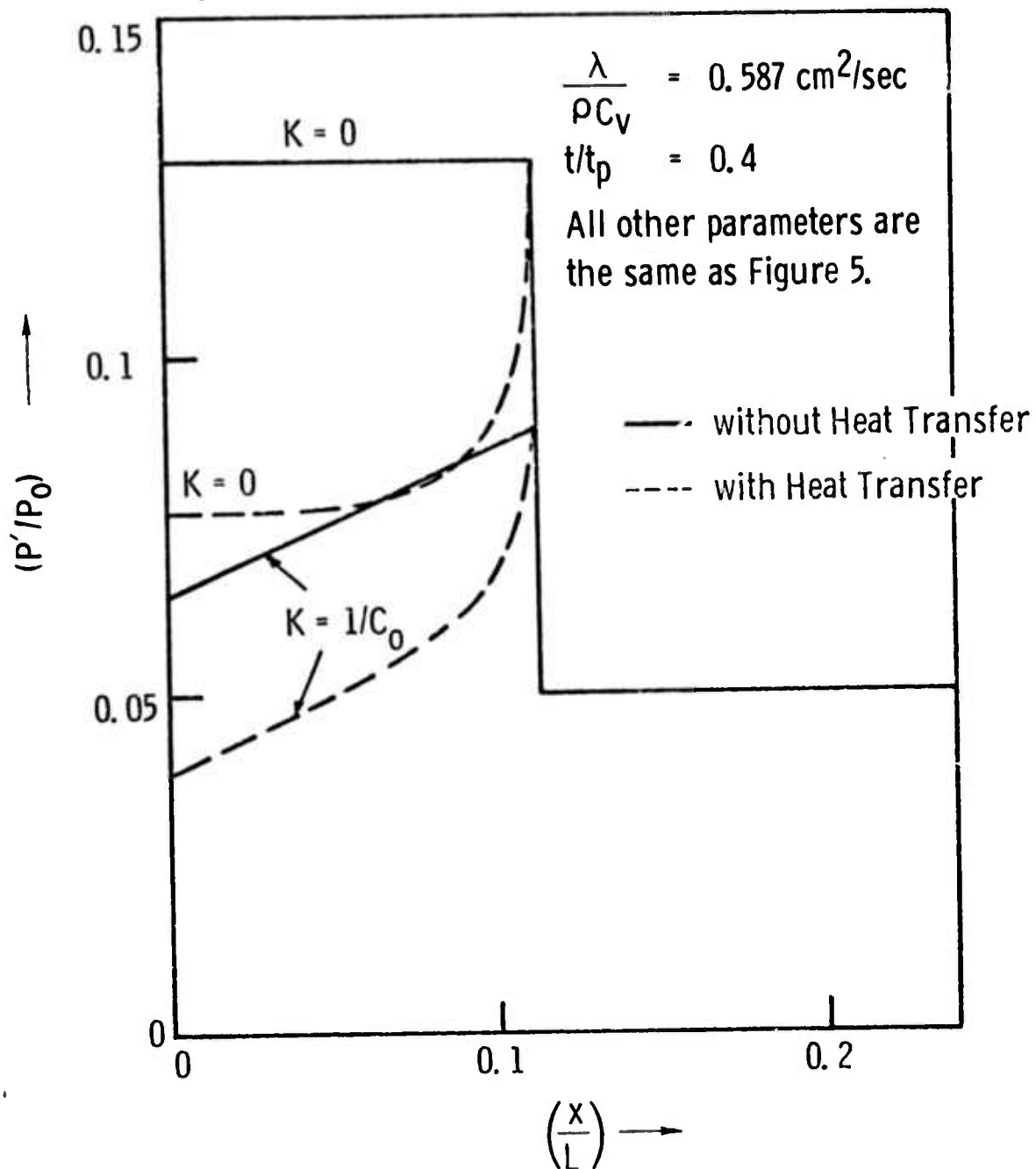


Figure 8. Typical cathode fall produced pressure profiles with and without heat transfer to the cathode.

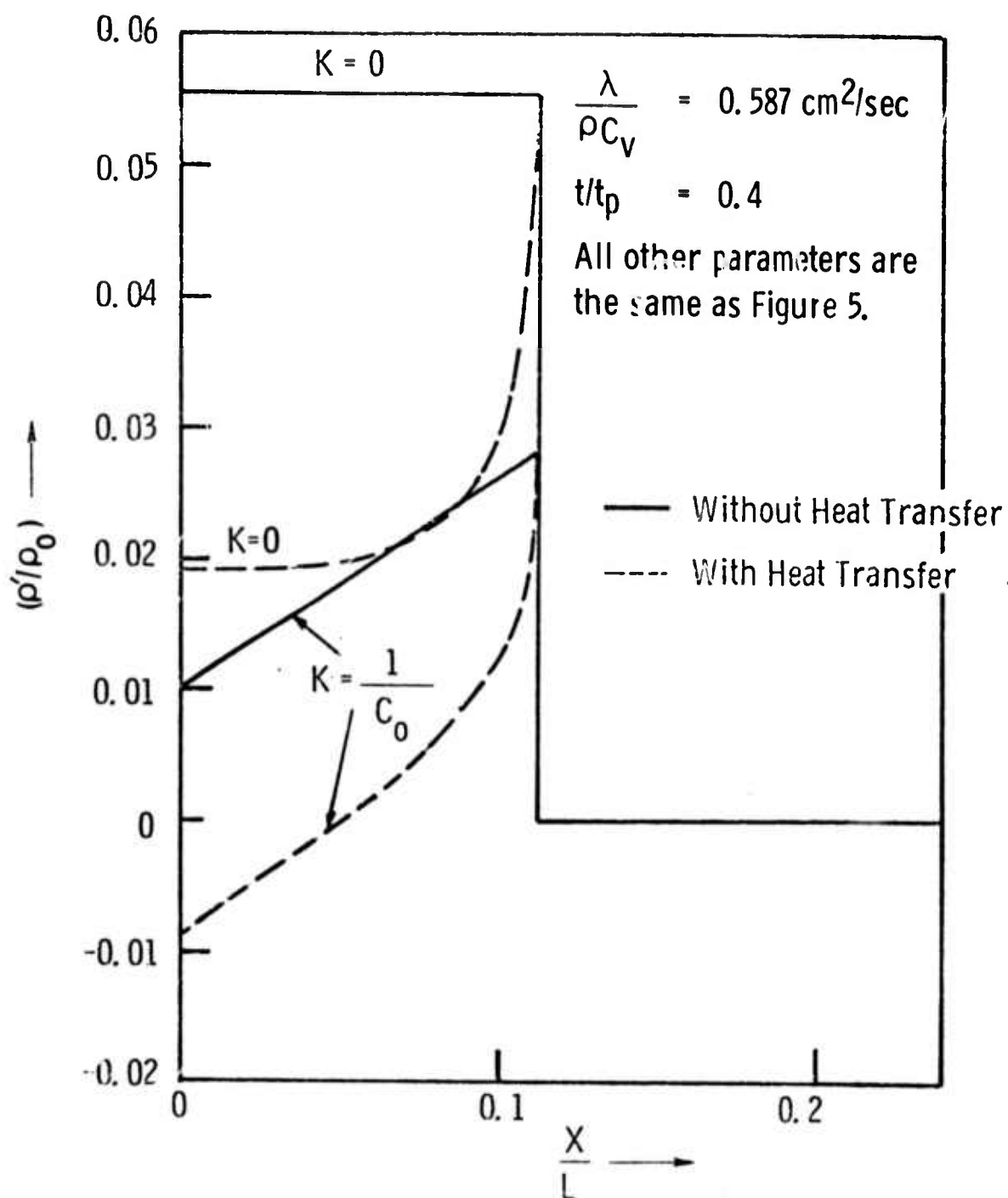


Figure 9. Typical cathode fall produced density profiles with and without the effects of heat transfer.

As time progresses ( $x/L$  becomes less in the figure), the magnitude of the wave decreases since more of the fall's energy is going into heating the cathode screen wires as opposed to mechanical work on the surrounding laser gas. After some time has passed ( $x/L = 0.05$  in the figure), a steady state has been established. The rates of cathode fall power input into cathode wire heating and into mechanical work on the gas are constant percentages and remain so for the duration of the discharge time period.

For the high porosity cathode case ( $K = 1/c$ ), the same qualitative effects occur except that the open area behind the cathode permits gas to flow from behind the compression wave, thus relieving the pressure and weakening the wave.

The important point to be drawn from the two figures (8 and 9) is that the slopes of the pressure behind the cathode wave are essentially identical for both the adiabatic and the finite cathode heat transfer cases after a short distance behind the compression wave front. In the case shown, this distance is roughly 5% of the total cavity length. The percentage of the total wave structure affected by cathode fall heat transfer is thus quite small and the majority of the wave pattern pressure and density gradients are identical for both the adiabatic and the finite heat transfer cases. This fortunate concurrence enables one to interpret the interferograms made of a pulsed EDL's cavity with the aid of the simpler adiabatic density wave analysis. Typical errors using the adiabatic analysis should be no greater than 1% or 2%. Inaccuracies incurred as a result of using this approach are thus much smaller than those occurring experimentally.

## 5.0 DETERMINATION OF BULK HEATING OF THE LASER PLASMA

Using the previously developed predictions of the density profiles in the laser cavity, prediction of the bulk heating of the laser plasma from experimental interferograms becomes a relatively straightforward task. The formal approach would be to differentiate every term of the adiabatic wave equation (equation (31)) with respect to  $x$ . Use of the adiabatic wave equation is justified by the previous section in which it was shown that cathode sheath heat transfer effects on the wave structure die out a short distance behind the compression wavefront.

Fortunately, it is not necessary to differentiate every term of (31). The equation is split into two parts: The first two terms describe the wave patterns caused by bulk heating. The second set of terms, preceded by the ratio,  $(Q_c^*/Q_h^*)$ , describes the wave pattern produced by the cathode fall heating. This second set of terms, if differentiated, cancel identically. This amounts to saying that the cathode fall heating causes a steep change in density profile and does not contribute to density gradients behind the compression wave front.

Performing the indicated differentiation, one obtains, for the cathode rarefaction wave:

$$d\rho^*/dx)_{\text{cathode}} = \frac{(\gamma - 1) \dot{Q}_h (Kc)}{\gamma c_p (1 + Kc)} \quad (45)$$

and, for the anode rarefaction wave:

$$\left( \frac{d\rho^*}{dx} \right)_{\text{anode}} = \frac{(\gamma - 1) \dot{Q}_h (K_a c)}{\gamma c_p (1 + K_a c)} \quad (46)$$

Bulk heating of the plasma is usually defined in terms of a percentage heating rate,  $\eta$ :

$$\eta = \dot{Q}_h / \dot{E}_{\text{in}} \quad (47)$$

Substituting this into (45) and (46) and noting that the cathode screen permeability is essentially that of the laser gas,  $1/c$ , we may write

$$\eta = \frac{\gamma c_p (1 + K_a c) \left( \frac{d\rho^*}{dx} \right)_{\text{anode}}}{(\gamma - 1) K_a c \dot{E}_{\text{in}}} = \frac{2\gamma c_p \left( \frac{d\rho^*}{dx} \right)_{\text{cathode}}}{(\gamma - 1) \dot{E}_{\text{in}}} \quad (48)$$

The effective heating rate,  $\eta$ , may thus be checked by both the cathode and the anode wave patterns providing that the acoustic permeability of the anode is sufficiently well known.

The cavity density gradient is most conveniently obtained from a Mach-Zehnder interferogram. With the aid of the interferogram, the density gradient is simply expressed as:

$$\frac{d\rho^*}{dx} = \frac{(\rho_s / \rho_o) \lambda \, dN/dx}{\Omega L} \quad (49)$$

where  $\rho_s$  is the density of the gas at standard conditions,  $\rho_o$  is the gas density at test conditions,  $L$  is the optical path length,  $\Omega$  is the Gladstone-Dale constant,  $\lambda$  is the wavelength of the light used, and  $dN/dx$  is the fringe gradient on the interferogram.

A Mach-Zehnder interferometer was set up to measure density waves in the Northrop 10 liter CO electric discharge laser. The setup is schematically shown in Figure 10. A ruby laser was used for making single and double pulsed, time resolved interferograms and a helium-neon laser, mounted on the ruby laser's optical axis, was used for system alignment. Firing of the ruby laser was correlated with firing of the CO laser by means of a fast rise time transducer fed with a fraction of the ruby laser's output. This trace was displayed in parallel with the sustainer current of the CO laser on a dual trace, high speed oscilloscope. Details of the experiment are described in Reference 6. Details of the Northrop 10 liter laser are reported in a previous semiannual technical report.<sup>5</sup>

Discharge measurements were made on pure  $N_2$ , CO/Ar mixes, and CO/ $N_2$  mixes. No optical extraction was made. Figure 11 plots observed fringe gradient behind the cathode wave as a function of input power for various combinations of sustainer voltages and gas mixtures. Figure 12 plots the derived heating rate,  $\eta$ .

From Figure 12, several important conclusions can be drawn regarding bulk heating of the laser discharge, at least in the absence of optical extraction.

1. At high sustainer voltages, the bulk heating rate of both  $N_2$  and the  $N_2$ /CO mixture depended very little upon input power for pumping rates above  $100 \text{ W/cm}^3$ .

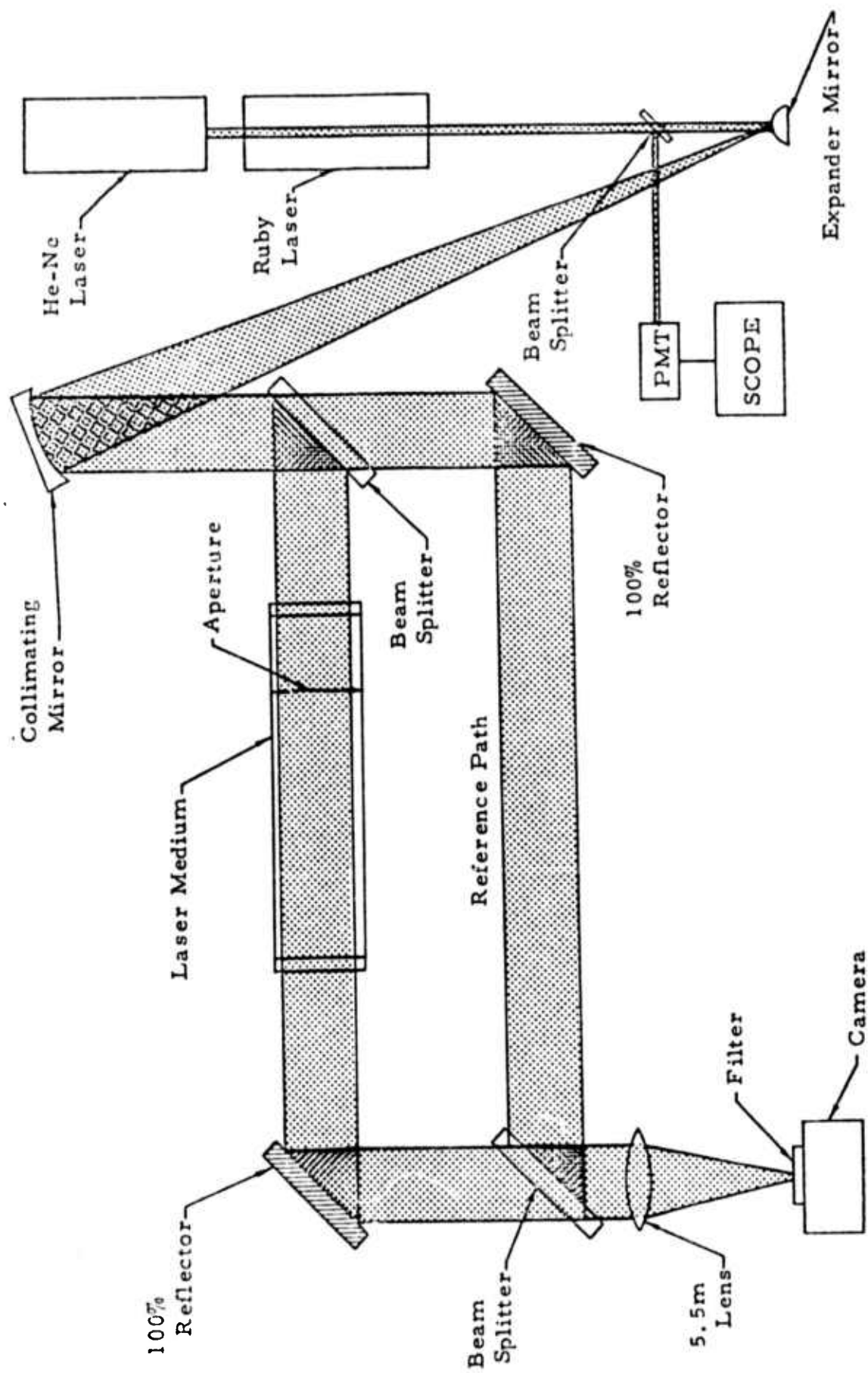


Figure 10. Interferometer configuration for studies of CO EDL density waves.

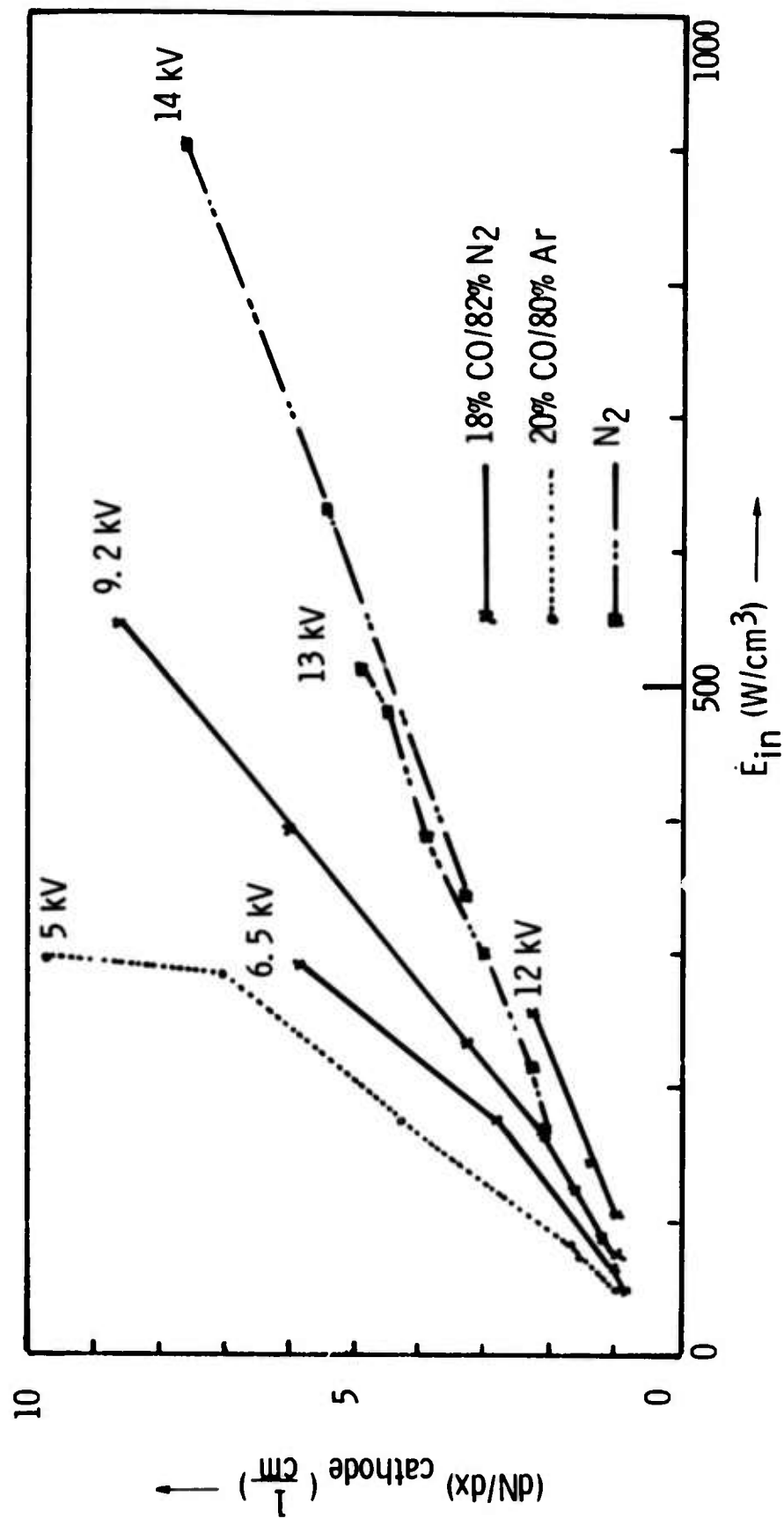


Figure 11. Experimentally determined fringe gradients from interferograms of the Northrop 10 liter CO electric discharge laser.  $P = 100$  Torr,  $T = 80^\circ\text{K}$ .

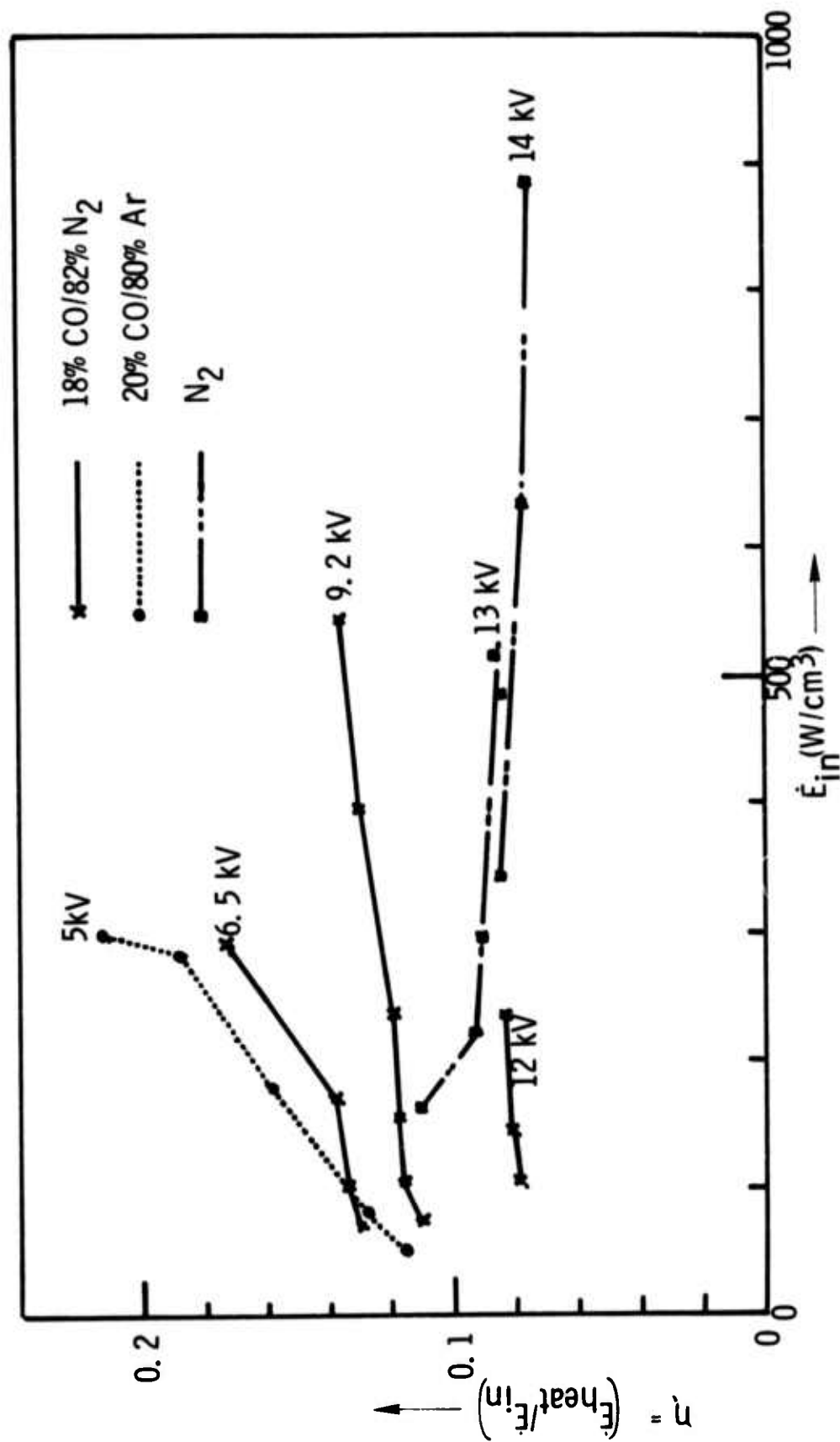


Figure 12. Experimentally determined heating rates in the Northrop 10 liter electric discharge CO laser.  $P = 100$  Torr,  $T = 80^\circ\text{K}$ .

2. At low sustainer voltages, heating rate does increase for increased pumping rate.
3. Over the limited range of similar voltages tested, the heating rate for  $N_2/CO$  does not appear to be appreciably different than that for  $N_2$  alone.
4. Similarly, for the limited range and low sustainer voltage tested, heating rates for  $CO/Ar$  and  $CO/N_2$  appear to be approximately the same.
5. Heating rate increases as sustainer voltage is lowered for the  $CO/N_2$  mixes.
6. In general, the heating rates for  $CO$  lasing gas mixtures appear to be quite low. In all cases, they are below 20% and, for maximum energy sustainer voltages (12-13 kV), heating rates are below 10%.

This last conclusion is particularly rewarding since it provides direct confirmation of the low heating rates predicted by the Northrop  $CO$  laser kinetics code and thus confirms the potential high efficiency of  $CO$  lasers in general.

6.0 REFERENCES

1. Avco Corporation, "Electron Injection Laser Technology Program, " (U), Interim Technical Report, Contract F29601-71-C-0084, October 1971, Secret.
2. Avco Corporation, "Electron Injection Laser Technology Program, " (U), Interim Technical Report, Contract F29601-71-C-0084, April 1972, Secret.
3. Avco Corporation, "Electron Injection Laser Technology Program, " (U), Interim Technical Report, Contract F29601-71-C-0084, August 1972, Secret.
4. D. Abhouse, M. Monsler, J. Reilly, J. Daugherty, W. Rosser, and J. Mangano, "A Theoretical and Experimental Medium Quality Investigation of Rapidly Pulsed E- Beam Sustainer Lasers, " (U), Proceedings of the Fifth Conference on Laser Technology, Vol. I, p. 85-128, April 1972, Secret.
5. G. L. McAllister, W. B. Lacina, D. K. Rice, and P. J. Mendoza, "High Power CO Laser Semiannual Technical Report," AD 780-265, May 1974.
6. A. L. Ward, "Calculation of Cathode-Fall Characteristics, J. Appl. Phys. 3, N9, September 1962.